

Using softer X-ray absorption spectroscopy to probe biological systems

Barak Akabayov,^a Christian J. Doonan,^b Ingrid J. Pickering,^b Graham N. George^{b*} and Irit Sagi^{a*}

^aDepartment of Structural Biology, The Weizmann Institute of Science, Rehovot 76100, Israel, and

^bDepartment of Geological Sciences, University of Saskatchewan, Saskatoon, Canada S7N 5E2.

E-mail: g.george@usask.ca, irit.sagi@weizmann.ac.il

Many inorganic species are now recognized as being essential for life, including many forms of sulfur, phosphate and numerous classes of metal ions. For example, recent progress in the fields of biochemistry and biology has pointed out the critical importance of sulfur in the biosynthesis of vital cofactors and active sites in proteins, and in the complex reaction mechanisms often involved. Special attention has also been drawn to the diverse roles of alkaline (Na⁺, K⁺) and alkaline earth (Mg²⁺, Ca²⁺) metal ions in mediating the activity of RNA, proteins and many processes in living cells. While the general effect of these ions in biology is mostly understood, information on their detailed role is deficient. Here the application of softer X-ray absorption spectroscopy (XAS) to probe the local structural and electronic environment of such ions within their biological complexes and during physiological reactions is discussed. In addition, the required experimental set-up and the difficulties associated with conducting softer XAS experiments on biological samples are presented.

1. Introduction

It is widely recognized that inorganic elements are essential for all forms of life. Although the majority of these elements are usually present in trace amounts, this does not undervalue their importance. Physiologically relevant inorganic compounds and elements include S²⁻/SO⁻/PO₄³⁻/CO₃²⁻/H₂O/Cl⁻, the alkaline (Na⁺, K⁺), alkaline earth (Mg²⁺, Ca²⁺) and transition metals (Mn, Fe, Co, Ni, Cu, Zn, Mo). Importantly, the effects of these inorganic elements on physiological process are exclusive and yet very diverse. For example, sulfur-based compounds are involved in several unusual reaction pathways under physiological conditions (Toohey, 1989). This is presumably due to the outstanding chemical versatility of sulfur. Interestingly, sulfur in its most oxidized form, namely sulfate, is of limited use to higher organisms except for sulfation and detoxification reactions. Rather, it is the lower oxidation states of sulfur [*e.g.* sulfenate (SO⁻)] that appear to be critical in nature for anabolic reactions (Beinert, 2000). Remarkably, nature utilizes sulfur in many fundamental biological reactions, *e.g.* reactive protein redox centers such as Fe–S clusters (Stiefel, 1996), disulfide bridges to fold proteins (Raines, 1997), enzyme catalysis and redox regulation (Claiborne *et al.*, 1999).

Other important inorganic elements belong to the family of metal ions. Noteworthy, distinct classes of metal ions exhibit

different biological roles. Alkaline metals (Na⁺, K⁺) are used as charge carriers, mediate osmotic and electrochemical gradients across cell membranes (MacKinnon, 2004) and are required for nerve function (Yogeeswari *et al.*, 2004). Recently, the contribution of potassium and sodium ions to the structural stability and function of the ribosome was pointed out by Klein *et al.* (2004). Specifically, 88 monovalent cations were identified in the crystal structure of the large ribosomal subunit, among which 86 were modeled as Na⁺ ions. Remarkably, Na⁺ and K⁺ ions were found to make many more contacts with functional groups on nucleotide bases than they do with the non-bridging phosphate oxygen atoms of the RNA backbone (Klein *et al.*, 2004).

Interestingly, the related class of alkaline earth metals exhibits somewhat different biological functions. Mg²⁺ and Ca²⁺ serve as enzyme and nucleic acid activators, and act as structure and conformational transition promoters (Bunick *et al.*, 2004; Massova *et al.*, 1998; Pyle, 2002) as well as Lewis acids in many cellular processes including RNA folding, ATP hydrolysis, blood clotting, biomineralization process and many more.

Lastly, over the years special attention has been given to the partnership between protein and transition metal ions [recently reviewed by Barondeau & Getzoff (2004)]. Transition metals mediate enzyme activity within protein catalytic sites *via* redox chemistry and acid–base catalysis. This is

achieved by subtle interactions between the diverse electronic properties of a given transition metal ion and the stability of protein conformations.

The diverse roles of inorganic elements in biology encouraged many research groups to characterize their novel interactions with protein and nucleic acids using protein crystallography. The vast advance in the field of protein crystallography has revealed vital new information concerning the nature of metal centers in various biological systems. The variability of oxidation state and coordination chemistry of metals result in novel metal–protein complexes and in many cases involves unique structural paradigms (Barondeau & Getzoff, 2004). Yet, the correlation between the structure of such reactive centers and their function is not trivial.

Apparently, rationalization of reaction mechanisms involving reactive metal centers in proteins requires (i) structural information at atomic resolution, and (ii) structural and electronic information on other reaction states and complexes. X-ray absorption spectroscopy (XAS) is capable of providing details of both physical structure and electronic structure. The X-ray absorption spectrum can be divided into two regions, the near-edge or X-ray absorption near-edge structure (XANES) and the extended X-ray absorption fine structure (EXAFS) regions. The former is the region within about 50 eV of the absorption edge, while the latter extends approximately 1 keV above the edge. The EXAFS can be analyzed to give structural information on the atomic neighborhood of the atom, while the near-edge is a sensitive indicator of electronic structure. The near-edge can often be complex to analyze quantitatively, and often a ‘fingerprint’ approach is most fruitful, in which spectra of a library of standard compounds are compared with the unknown. EXAFS, on the other hand, can be readily analyzed to provide quantitative structural information. It has been demonstrated that the combination of high-resolution crystallographic information and EXAFS is a powerful approach for studying the structure–function relationships in metalloproteins, particularly when subtle structural changes are associated with a chemical reaction (Cheung *et al.*, 2000). This approach, which makes direct use of three-dimensional information from protein crystal structures in the analysis of EXAFS data, is likely to be of most interest in cases where crystallographic information is available for some state of a protein but not for others. In this respect, the advantages of combining protein crystallography with spectroscopic studies [*e.g.* electron paramagnetic resonance (EPR), XAS] on biological samples are evident. The latter are crucial to the assignment of an oxidation state to the metal atom and a determination of the electronic structure of the metal center that is often optimized with respect to the biological function of the macromolecule.

Advances in X-ray fluorescence detectors, in beamline technology and in XAS theory have allowed high-quality EXAFS data to be measured and analyzed on samples with low metal content (Cheung *et al.*, 1999; Fischetti *et al.*, 2004). However, the acquisition of high-quality *K*-edge XAS data of biological samples (bioXAS) has proven feasible mostly for transition-metal–protein sites (*e.g.* Mn, Fe, Ni, Cu, Zn, Mo).

XAS at the *K*-edges of such physiological transition metals utilizes X-rays in the range 6–20 keV. This requires a relatively simple experimental set-up in which equipment is operated at atmospheric pressures, currently adopted in many dedicated bioXAS synchrotron beamlines. In contrast, probing the local environment of low-*Z* number elements, *e.g.* S, P, Na⁺, K⁺, Mg²⁺, Ca²⁺, by XAS requires the use of softer X-rays (1–4 keV). This is non-trivial since such experiments require a special beamline set-up (*e.g.* windowless beamlines, vacuum conditions and helium paths) and tailored built-in detection systems. Nevertheless, as described above, application of softer XAS to biological systems promises to yield novel mechanistic information on the structure and electronics of low-*Z* inorganic elements coordinated to reactive protein and nucleic acid sites.

Here we discuss the importance of using softer bioXAS to probe the interactions of low-*Z* inorganic elements with biological systems. As an example we describe novel bioXAS experiments using Al and S *K*-edge spectroscopy and we demonstrate the role of Mg²⁺ ions in RNA folding and in enzyme catalysis. In addition, we will discuss the technical difficulties associated with softer bioXAS data acquisition and experimental set-up.

2. Aluminium *K*-edge XAS

Unlike its neighbor magnesium (see below), aluminium has no known biological function, and its biological disposition appears to be confined to toxic effects. Aluminium is a major constituent in rocks and soils, but it normally exists as a stable complex with oxygen and silicate in neutral and weakly acidic soil. In naturally acidic soils, or in the presence of so-called ‘acid rain’ from sulfur dioxide emissions, toxic levels of Al³⁺ can be present. These adversely affect plant growth by inhibiting root growth and limiting subsequent uptake of water and nutrients (Kochian, 1995; Matsumoto, 2000). It has been estimated that some 40% of the soil on earth is acidic, and unavailable for agriculture essentially because of aluminium toxicity (von Uexkull & Mutert, 1995) and, because of this, efforts are underway to develop crop plants that are resistant to the toxic effects of aluminium (Delhaize *et al.*, 2004). In animals, Al³⁺ absorption is poor, but once absorbed it can cross the blood brain barrier and reach the brain (Julka *et al.*, 1996; Yomoto *et al.*, 1997). Once there it exhibits neurotoxic effects (Julka *et al.*, 1996; Yomoto *et al.*, 1997), and has been shown to trigger neuronal apoptosis (Toimela & Tahti, 2004). Evidence exists that it plays a role in a variety of neurodegenerative human diseases, such as Alzheimer’s disease (Jellinger & Bancher, 1998), amyotrophic lateral sclerosis (Yasui *et al.*, 1991), Parkinson’s disease (Hirsch *et al.*, 1991) and dialysis dementure (Flendrig *et al.*, 1976). Despite its biological importance, we remain ignorant of the molecular mechanisms by which aluminium exerts its toxic effects on plants and on animals. One reason for this is that aluminium, like magnesium, can be regarded as a ‘spectroscopically quiet’ element (Penner-Hahn, 2004) in that there are few convenient spectroscopic probes. ²⁷Al nuclear magnetic resonance

(NMR) spectroscopy can be used as a probe of the coordination environment of the metal. Al *K*-edge X-ray absorption spectroscopy provides a potentially very powerful tool for providing structural information on aluminium in biological systems. The near-edge portion of the spectrum is very sensitive to the coordinating environment, and in many cases may be sufficient in providing a fingerprint-style speciation of the coordination environment. Fig. 1 shows an example in which a series of different octahedral aluminium species coordinated with oxygen ligands give quite distinct spectra, illustrating the sensitivity to the specific metal coordination environment.

3. Sulfur *K*-edge XAS

Sulfur is another spectroscopically quiet element in that it lacks a well established spectroscopic probe. The low natural abundance, weak magnetic moment and significant nuclear electric quadrupole moment of ^{33}S combine to make ^{33}S NMR challenging, and it is not widely used. In recent years the richness of the sulfur *K*-edge X-ray absorption near-edge spectroscopy has become apparent, with a chemical shift range spanning more than 14 eV (Fig. 2). It has been successfully used in speciating complex mixtures of sulfur in fossil fuels (e.g. George & Gorbaty, 1989), soils (Morra *et al.*, 1997), organic marine sediments (Vairavamurthy *et al.*, 1994), as a probe of the electronic structure of sulfur-containing metalloproteins (e.g. Dey *et al.*, 2004; George *et al.*, 1996, 2000; Shadle *et al.*, 1993; Williams *et al.*, 1997; Solomon *et al.*, 2005), and the blood biochemistry of ascidians (Frank *et al.*, 1999). The variability of the near-edge spectrum is such that it is even

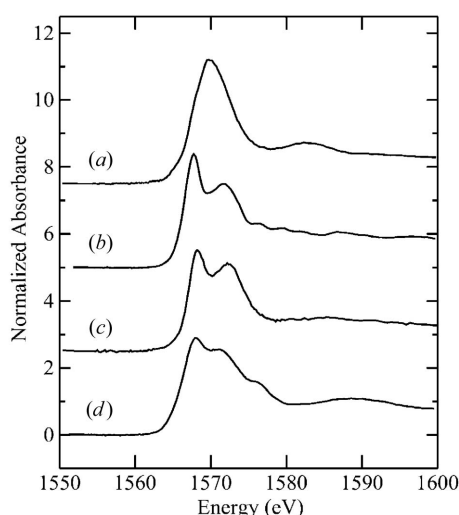


Figure 1

X-ray absorption near-edge spectra of approximately octahedrally coordinated aluminium oxygen species, illustrating the sensitivity of the near-edge spectra to coordination environment. The data were recorded on SSRL's beamline 3-3 (JUMBO) using a YB₆₆ double-crystal monochromator (note that this instrument has now been decommissioned). All spectra are of solids (not solutions) recorded using total electron yield under a vacuum. (a) Aluminium acetylacetonate, (b) α -alumina (Al_2O_3), (c) alum [$\text{KAl}(\text{SO}_4)_2 \cdot 12\text{H}_2\text{O}$] and (d) kyanite (Al_2SiO_5).

possible to deconvolute the complex mixtures observed in living tissues (Pickering *et al.*, 1998, 1999, 2001; Sneed *et al.*, 2004; Yu *et al.*, 2001).

4. Arsenic and selenium *L*-edge XAS

The *K*-edges of arsenic and selenium have proved useful in the speciation of these biologically important metalloids (e.g. Pickering *et al.*, 1999). The *L*-edges, however, have been relatively little investigated, and in fact show a rich near-edge spectroscopy which may prove to be more sensitive to chemical type than the *K*-edge. Fig. 3 illustrates the sensitivity of the selenium *L* near-edge spectra to chemical type.

5. The role of alkaline and alkaline earth metals in RNA folding

Structured RNA molecules play key roles in execution and control of many biological processes, such as protein transport, RNA splicing, polypeptide synthesis and its regulation (Cech, 2002; Collins & Guthrie, 2000; Faustino & Cooper,

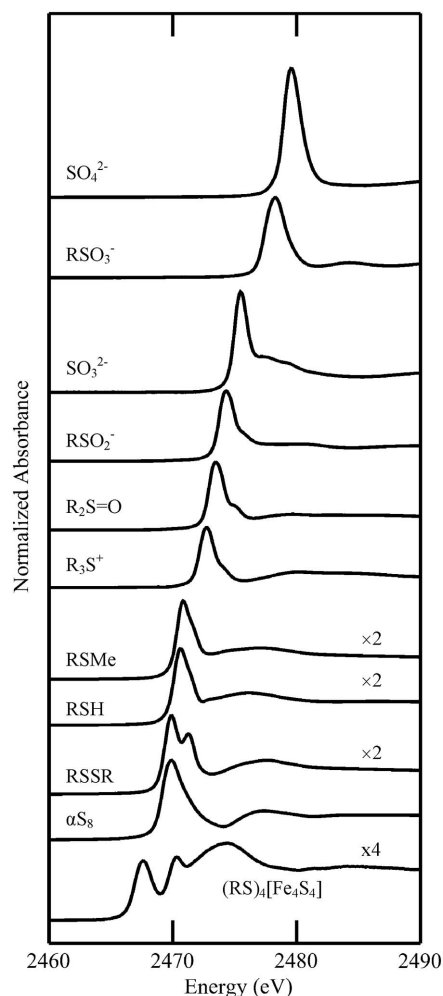


Figure 2

X-ray absorption near-edge spectra of representative sulfur species in aqueous solution at or near pH 7.0. All spectra were normalized to the height of the edge jump after background removal.

2003; Gesteland *et al.*, 1999; Steitz & Moor, 2003). The importance of RNA has been recently highlighted with the discovery of post-transcriptional gene silencing mediated by non-coding RNAs (RNA interference) (Denli & Hannon, 2003). These processes are facilitated by the multifunctional nature of RNA molecules, which act as structural skeletons,

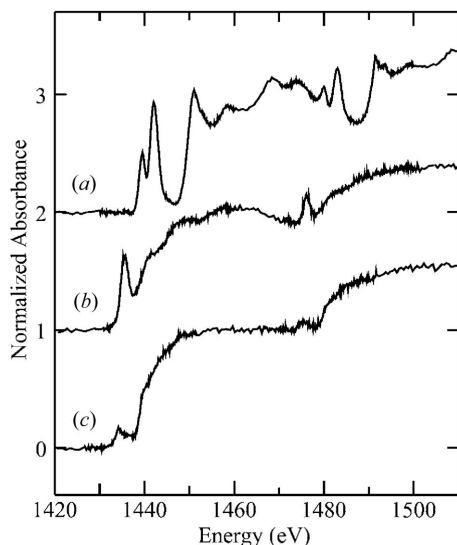


Figure 3 Selenium L -edge X-ray absorption near-edge spectra of a selection of biologically important species. (a) Selenate (Na_2SeO_4), (b) selenomethionene and (c) α -selenium. The spectra were recorded using the same experimental set-up as those of Fig. 1, and the energy range includes both the L_{III} and L_{II} absorption edges.

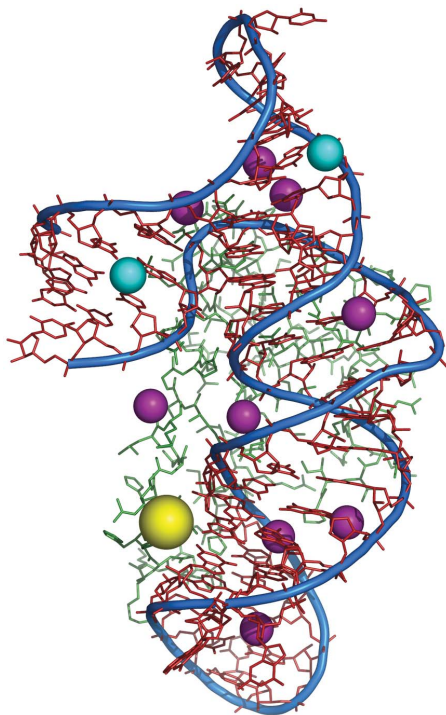


Figure 4 High-resolution crystal structure of ribosomal S15 protein bound to its rRNA site (PDB code 1DK1). The spheres are modeled as metal ions: purple spheres, Mg^{2+} ; blue, Na^+ ; yellow, K^+ . [Adopted from (Pyle, 2002).]

molecular switches or catalysts, depending on their structure. Stable and ‘functionally correct’ RNA folds form by specific and non-specific interactions *in cis*, as well as with certain classes of metal ions (K^+ , Na^+ , Mg^{2+}), and *via* the interaction of RNA with different protein factors acting as RNA chaperones (Herschlag, 1995; Lorsch, 2002; Pyle, 2002).

Fig. 4 shows the high-resolution crystal structure of the S15 ribosomal protein (presented in ribbon) bound to its 16S ribosomal RNA (rRNA) site (PDB code 1DK1). The RNA fold is heavily supported by the interaction of alkaline and alkaline earth metal ions with the RNA backbone. Structured RNA molecules are complex three-dimensional objects, stabilized by hundreds of canonical (Watson–Crick) and non-canonical bonds, which form sequentially as the molecule folds (Woodson, 2000). As a result, RNAs are prone to be trapped kinetically in stable structures that can persist for long periods of time (Treiber & Williamson, 1999). The basic question relevant to this phenomenon is how can large RNA molecules fold into their unique functional structure and not be trapped in a ‘misfolded’ structure? The answer to this question is partially explained by the dynamic involvement of RNA chaperones in the form of proteins or chemical agents (*e.g.* metal ions), and by the sequential nature of the folding process, which can guide the folding process toward its proper state.

Fig. 5 illustrates the effects that different Mg^{2+} concentrations have upon the structure of an RNA molecule. In this experiment, an 80 base-long 23S rRNA fragment was incubated with different Mg^{2+} concentrations (0–100 μM) and measured by circular dichroism (CD) in the far UV range. Titration of the RNA solution with increasing amounts of Mg^{2+} ions drives the RNA molecule from its partially unfolded to folded state. The CD spectra of the renatured 80 *mer* RNA exhibit major transitions at 270 nm (Fig. 5) caused by π – π^* electronic transitions in the stacked planar bases of the RNA (Johnson, 1992). Specifically, the asymmetric 3'-endo sugar ring effects these transitions. Spectral changes observed at 210 nm are attributed to formation of A-helix structure (in the RNA stem). The gradual increase in the peak amplitude at 270 nm directly correlates with the degree of RNA folding.

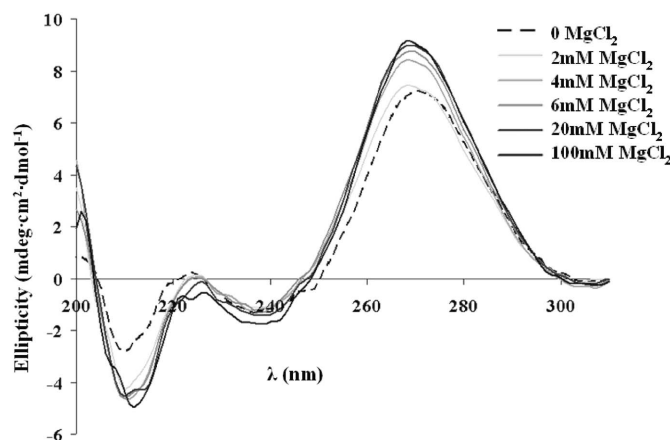


Figure 5 CD measurements of 80 base rRNA fragment as a function of Mg^{2+} ions.

Reduction in ellipticity is observed at 270 nm at elevated temperatures (data not shown). Similar results were detected in other RNA systems (group I introns) by monitoring the CD spectra during urea titration (Su *et al.*, 2003). Spectral changes at 270 nm suggest modifications of the base-stacking content at the RNA loop regions (Johnson, 1992). In contrast, the stem structure of the RNA remained unchanged after the initial addition of Mg^{2+} ions. These results demonstrate that Mg^{2+} ions serve as chemical chaperones in the process of RNA folding of a given RNA molecule.

Yet, CD experiments conducted under these reaction conditions do not contain quantitative information on the nature of the folded state, the number of coordinating metal ions and their role in active folding of RNA. Similarly, designing bioXAS experiments using simple Mg^{2+} titration experiments will most likely yield limited averaged structural information on an ensemble of Mg^{2+} coordination sites. Therefore, structural characterization of individual metal sites in pathways of RNA folding and catalysis requires the utilization of monovalent metal ions and advanced 'RNA rescue experiments' (Pyle, 2002).

The monovalent K^+ and Na^+ ions are known to play a variety of roles in the folding of complex RNA structures and in the catalytic activity of ribozymes (Draper, 2004). These metals can be thermodynamically bound at specific sites (site-bound), or kinetically labile (diffuse or delocalized) (Misra & Draper, 1998). In addition, site-bound metal ions can remain fully hydrated (outer sphere), or can become partially or fully dehydrated (inner sphere). Monovalent ions (K^+ , Na^+) have also been shown to play important roles in both the secondary and tertiary folding of RNAs (Misra & Draper, 1998; Pyle, 2002). Overcoming a rough folding landscape (formed by kinetically trapped RNA) strictly depends on critical concentrations of Mg^{2+} ions and the timing of their addition to the reaction mixture. This may be utilized to monitor specific Mg^{2+} ion sites on partially folded RNA fragments (with monovalent ions) by softer bioXAS.

Probing the mechanistic role and structure of specific metal sites during RNA folding and catalysis is often studied by chemical mutagenesis experiments such as transition metal rescue experiments (Pyle, 2002). These experimental procedures require the replacement of the 3'-hydroxyl leaving group at the scissile linkage with a 3'-thiol group. The chemically modified site has a greater affinity to transition metals such as Mn^{2+} , Cd^{2+} and Zn^{2+} over Mg^{2+} . Therefore the stoichiometric addition of these metals to partially folded and inactive ribozyme rescues its catalytic activity (Piccirilli *et al.*, 1993). Prior studies of the metal ion dependence on the self-cleavage reaction of the HDV genomic ribozyme led to a mechanistic framework in which the ribozyme can self-cleave by multiple Mg^{2+} ion-independent and ion-dependent channels (pathways) (Nakano *et al.*, 2001), which either involve metal ions or do not. In particular, channel 2 involves cleavage in the presence of a structural Mg^{2+} ion without participation of a catalytic divalent metal ion, while channel 3 involves both structural and catalytic Mg^{2+} ions. Recent studies support the existence of two different classes of metal ion sites on the

ribozyme: a structural site that is inner sphere with a major electrostatic component and a preference for Mg^{2+} , and a weak catalytic site that is outer sphere with little preference for a specific divalent ion.

Attempts to characterize RNA-metal reactive sites in ribozymes have been made using EPR spectroscopy on Mn-substituted sites (Schiemann *et al.*, 2003). In many cases such metal-substitution studies result in partial inactivation of the biological systems. Therefore, conducting bioXAS measurements of intact alkaline and alkaline earth metals may utilize the use of chemically modified RNA molecules, partially folded with transition metal ions. Such experiments have the potential to provide a direct experimental approach to the study of the solution structure and electronics of alkaline and alkaline earth metals during stages of RNA folding and catalysis. Importantly, such experiments would need to be carried out in stoichiometric amounts of RNA-metal using mM concentrations. This can be achieved using large-scale *in vitro* transcription methods for RNA synthesis (Milligan *et al.*, 1987). In this approach the synthesis of small RNAs of defined length and sequence is carried out using T7 RNA polymerase and templates of synthetic DNA which contain the T7 promoter.

6. The role of alkaline and alkaline earth metal ions in mediating enzymatic catalysis of adenosine triphosphate (ATP) hydrolysis

The application of softer bioXAS measurements of reactive alkaline and alkaline earth metal sites may also be extended to many protein systems. For example, most biological systems, which preferentially bind ATP and use its free energy of hydrolysis to drive reactions, utilize metal ions as cofactors. Hydrolysis of ATP is used to drive countless biochemical reactions, including many that are not phosphorylations. It is a direct source of energy for cell motility, muscle contraction and the specific transport of substances across membranes. These enzymatic reactions often utilize K^+ , Na^+ and Mg^{2+} ions for effective catalysis and regulation. As shown in protein crystal structures available on many enzyme-ATP/ADP complexes, these ions coordinate both the backbone phosphates of ATP and protein side chains (Toyoshima *et al.*, 2004).

The detailed role of K^+ , Na^+ and Mg^{2+} ions in mediating enzyme catalysis is unknown. This is in part due to the lack of systematic spectroscopic analysis of these protein-metal sites. Importantly, in most enzymatic reactions, K^+ , Na^+ and Mg^{2+} are considered as incorporated reaction cofactors and not as intrinsic catalytic metal sites (such as transition metal ions). However, evidence for their direct participation in enzyme catalysis is emerging (Galburt *et al.*, 1999).

To assess the role of Mg^{2+} during enzymatic catalysis we conducted XAS measurements on the *E. coli* RNA helicase DbpA. The family of RNA helicases are ATP-dependent enzymes, which unwind duplex RNA regions (Rocak & Linder, 2004). These enzymes carry out their function by utilizing ATP hydrolysis to disrupt hydrogen bonding in

duplex RNA regions (Henn *et al.*, 2001). This reaction is mediated by Mg^{2+} ions which coordinate both ATP and protein side chains (Fig. 6*a*). Importantly, substitution of Mg^{2+} by Mn^{2+} ions retains full enzyme activity. Therefore, the Mn-substituted form of DbpA may be used for systematic spectroscopic analysis of the metal site during stages of the enzymatic reaction in solution. Figs. 6*(b)* and 6*(c)* show normalized Mn *K*-edge spectra of Mn-substituted DbpA in four different states of the enzyme. Specifically we have examined the metal binding site in DbpA when the enzyme is bound to (i) non-hydrolysable ATP analogue (ATP γ S), (ii) ADP, (iii) RNA-ATP γ S and (iv) RNA-ADP. Spectral changes in the shape of distinct transitions accommodated by significant changes in edge energy are observed in the various spectra. Such spectral changes in pre-edge and post-edge transitions are correlated with structural changes of the nearest coordination shell of the metal ion (Kleinfeld *et al.*, 2003). Importantly, these changes in coordination environment of the metal ion may be correlated with conformational transitions of the protein in these enzyme states (Henn *et al.*, 2002). These results suggest that the Mg^{2+} ions in ATP-dependent helicases participate in the reaction mechanism by mediating protein conformational transitions required for effective catalysis.

The sections above describe the increasing interest in many fields of biology to characterize the interaction of low-*Z* inorganic elements with proteins and nucleic acids by spectroscopic methods. Using softer bioXAS measurements to characterize these reactive sites during physiological reaction may provide critical mechanistic information. Yet, as we have mentioned above, application of XAS procedures on dilute samples using soft X-rays is not straightforward. Below we describe some of the specific experimental factors that need to be considered.

7. Experimental aspects

7.1. Attenuation of the X-ray beam

Biological X-ray absorption spectroscopy generally requires that aqueous solutions be studied. This requirement makes the vacuum environment of most soft X-ray beamlines undesirable or even unworkable. Thus, at low X-ray energies the major experimental difficulties arise from attenuation of the X-ray beam by the atmosphere (if present) and by X-ray windows. Indeed, almost all of the experimental difficulties considered here stem from X-ray beam attenuation problems. Fig. 7 shows the percentage transmission of various materials *versus* X-ray energy. It can be seen that beam attenuation problems are severe, especially for the lighter elements. A typical set-up for experiments at the sulfur *K*-edge (for example) might involve a helium flight path, with polypropylene windows, such as that shown in Fig. 8. The sample can either be maintained in an atmosphere of air (1 mm pathlength) or N_2 for oxygen-sensitive samples. For work in solution, maintaining the sample in helium is undesirable because of rapid diffusion of helium through the necessarily thin X-ray windows containing the sample (*e.g.* 6 μ m poly-

propylene). This causes helium bubbles to form in the solution sample that interfere with data collection. Furthermore, if helium atmospheres are used, then the helium flight path must be purged to remove air following every sample change. This is cumbersome and adds 20–30 min to the total time required for each sample. For softer X-rays, for example, at the Mg *K*-edge, vacuum beamlines probably cannot be avoided, and solution cells with thin vacuum-compatible windows must be used. At these energies, experimental difficulties multiply in proportion to the X-ray attenuations shown in Fig. 8.

7.2. Detectors

An additional experimental difficulty at low energies concerns detectors. For hard X-ray biological XAS the use of energy-dispersive array detectors (Friedrich *et al.*, 1998) has become standard practice for facilitating separation of signal (typically the *K α* fluorescence of a transition metal ion) and background radiation (typically elastic and inelastic scattered X-rays). With copper *K*-edge measurements, for example, the Cu *K α* emission is more than 900 eV lower in energy than the absorption edge (and the elastic scatter), and about 700 eV lower in energy than the start of the scan. The typical operating resolution of solid-state detectors is around 300 eV, with a maximum achievable resolution of about 150 eV (at low count rates). This means that excellent background removal can be achieved with first transition metal ions. Unfortunately, this is not the case with soft X-ray absorption spectra of elements of biological interest. At the sulfur *K*-edge, for example, the *K α* fluorescence is separated by only 160 eV from the edge position, at the Mg *K*-edge this separation is decreased to only 50 eV, and at the Na *K*-edge it is a mere 30 eV. Thus, solid-state detectors are unable to reject scattered radiation in these experiments, although removal of fluorescence from other sample components may still be an advantage. In general, for most of the soft X-ray work to date, integrating-type detectors are used, and the concentration limits for soft X-rays are effectively higher.

7.3. Sensitivity

The lower concentration limit of bioXAS critically depends upon a number of factors, including beam stability, X-ray flux and the nature of the detector used. For EXAFS spectra the sensitivity required is generally around a factor of ten greater than for near-edge studies. In the hard X-ray regime, using a modern high-intensity beamline with excellent beam stability, and state-of-the-art detectors, it has recently been proven possible to measure adequate signal-to-noise spectra at very low concentrations ($\sim 1 \mu$ M) (Harris *et al.*, 2003). In general, however, most experimental set-ups are incapable of such low-concentration measurements, and close to 1 mM concentrations are required for EXAFS, and about 0.1 mM for near-edge spectra. At softer energies the sensitivity is worse, owing to pathlength effects and lower fluorescence yields, and the lowest concentrations that can be investigated are correspondingly increased. At the sulfur *K*-edge, and using the experimental set-up shown in Fig. 8, adequate near-edge

softer X-rays

spectra could be obtained on samples containing ~ 1 mM sulfur, but a more useful lower limit would be about 10 mM. At the Mg and Al *K*-edges the sensitivity is expected to be poorer still, but at present insufficient work has been done to estimate lower limits for concentrations. Sensitivities are expected to increase as detector and beamline technology improves.

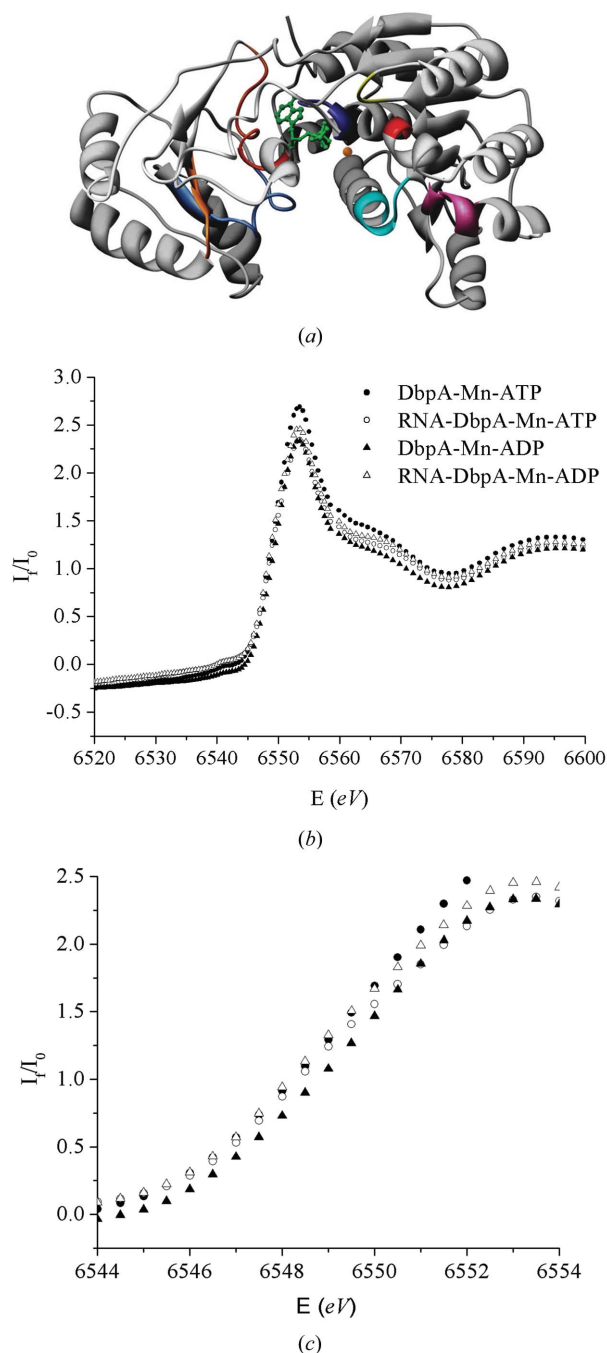


Figure 6
 (a) The core structure of the *E. coli* RNA helicase DbpA. The conserved and functional protein domains are highlighted in blue, purple, red, yellow, brown and light blue. Mg^{2+} (designated as a brown sphere) is bound to ATP (green). (b) Mn *K*-edge spectra of Mn-substituted DbpA bound to ATP γ S, ADP, RNA-ATP γ S and RNA-ADP. (c) Expanded view of the pre-edge spectra of (b) (6544–6552 eV).

7.4. Radiation damage and cryoprotection

Radiation damage is a great concern at soft X-ray energies. This is because the entire X-ray beam is absorbed by the sample in a very short pathlength (e.g. see Fig. 7) and the power deposited into the spectroscopically active volume of the sample is much greater than at higher X-ray energies

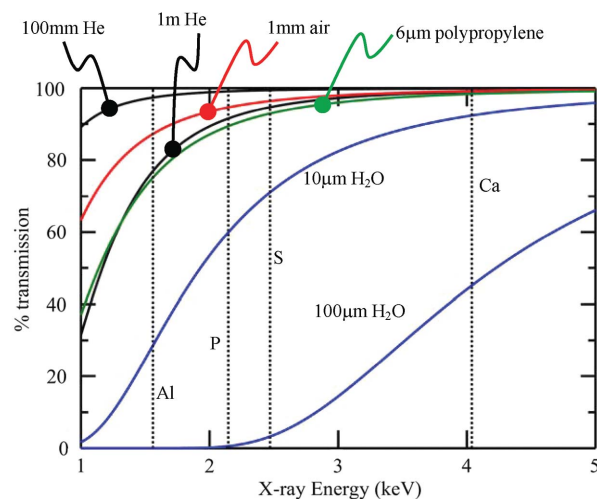


Figure 7
 Percentage transmission of X-ray beam versus energy for various materials and pathlengths.

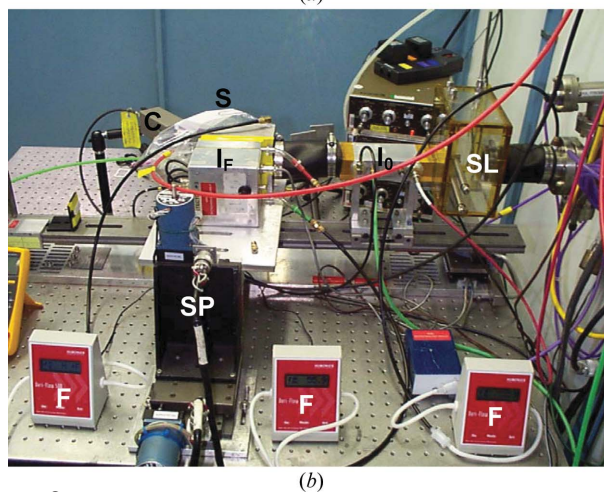
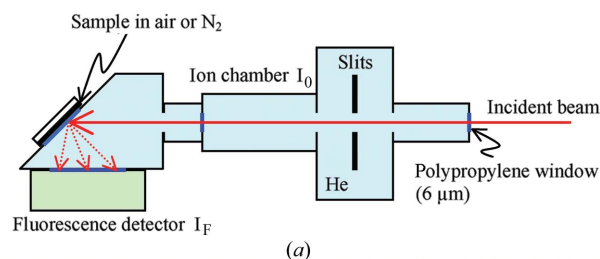


Figure 8
 (a) Schematic diagram of the experimental set-up for soft X-ray biological XAS on SSRL's beamline 6-2. A plan view of the set-up is shown. (b) Photograph of the actual set-up. Shown in the photograph are slits (SL), ion chamber (I_0), fluorescence detector (I_F), sample compartment (S), video camera for sample monitoring (C), sample positioner (SP) and digital flow meters (F) for monitoring the ion chamber, fluorescence detector and flight path gases. Not shown is an oxygen sensor, used to quantitatively monitor the air content in the flight path.

where the beam is more penetrating. The use of cryostats is becoming standard practice for hard X-ray biological X-ray absorption spectroscopy. Typically a liquid-helium flow cryostat operating at 10 K might be used (this is standard equipment on SSRL's XAS beamlines, for example). Radiation damage is usually manifest in the form of photoreduction, and is very difficult to predict, some samples being more susceptible than others. For susceptible samples, liquid-nitrogen temperatures generally provide insufficient protection, and liquid helium is therefore required. The experimental requirement for thin windows means that cryostats are difficult to design and operate at soft X-ray energies, and in most cases they are cumbersome devices whose operation is fraught with difficulties. The development of a useful well designed soft X-ray cryostat system would be a major contribution towards a more usable softer bioXAS.

7.5. Beamlines

The most significant recent technological advance in dedicated soft X-ray fluorescence beamline design has been the development of monochromator optics. Double-crystal monochromators (DCM) have traditionally employed germanium or silicon owing to their high resistance to radiation damage. A distinct limitation of these crystals for soft XAS is that the *d*-spacings of these crystals only permit a usable operating energy range down to approximately 2 keV. As a consequence, the *K*-edges and *L*-edges of some biologically pertinent elements are rendered inaccessible. A subtle increase in energy range is afforded by InSb crystals [the InSb(111) cut encompasses an energy range of 1683–11910 eV] which possess similar physical properties to silicon and germanium. Insulating crystals such as quartz, beryl and α -SiO₂ are effective between energies of 1–2 keV, and energies down to approximately 500 eV can be achieved by Na β -alumina and organic phthalate salts (*e.g.* KAP and RAP); however, their facile deterioration owing to high radiation loads is a considerable disadvantage for routine spectroscopy. The most satisfactory DCMs that cover the 1–2 keV energy range utilize a YB₆₆ crystal set (Wong *et al.*, 1994). These semiconducting artificial crystals possess a *2d* spacing of 11.72 Å for the (400) plane, resulting in a spectroscopically viable energy range of 1074–7600 eV. In addition,

Table 1

A partial list of beamlines with capability in the 1–4 keV range and general XAS beamlines that routinely operate above 2 keV.

DCM, double-crystal monochromator. PGM, plane-grating monochromator. VLS, variable line spacing. SGM, spherical-grating monochromator. Beamlines for which the information in the table is not available are not included

Location	Beamline	Energy range (eV)	Monochromator optics	
Photon Factory, Tsukuba, Japan	BL-2A	1740–5000	DCM, Si(111), InSb(111)	
	BL-2C	250–1500	Self-focusing PGM	
	BL-7A	100–1500	Grazing-incidence VLS PGM	
	BL-8A	38–2300	PGM (SX-700)	
	BL-8B	1700–2100	DCM, Si(111), InSb(111)	
	BL-9A	2200–15000	DCM, Si(111)	
	BL-11A	70–1900	Grazing-incidence VLS PGM	
	BL-11B	1760–3910	DCM, Ge(111), InSb(111)	
	European Synchrotron Radiation Facility, Grenoble, France	ID1	2000–42000	DCM, Si(111), Si(311)
		ID8	400–1600	SGM (Dragon-type)
		ID12	500–1600	SGM (Dragon) DCM Si(111)
		3000–22000		
ID21-STXM		200–8000	DCM Si(111) > 2eV /	
-TXM		2500–8000	PGM < 2 eV channel-cut monochromator	
ID26		2400–27000	DCM, Si(111), Si(220)	
BL15XU		500–60000	YB ₆₆ (1–2 keV), Si(111) (2–20 keV)	
BL17SU		100–3000	VLS PGM	
BL23SU		500–1500	VLS PGM	
BL25SU		220–2000	VLS PGM	
BL27SU	170–2800	VLS PGM		
MAX-Lab, Lund University, Sweden	I311	30–1500	PGM (SX-700)	
	I411	50–1500	PGM (SX-700)	
	I511-1	100–1500	PGM (SX-700)	
	I811	2400–20000	DCM, Si(111), Si(311)	
	BESSY, Berlin, Germany	ID-05-1	60–1300	PGM
ID-05-2		20–1900	PGM	
ID-07-1		20–1900	PGM	
ID-09-1		85–1600	SGM	
ID-09-2		85–1600	PGM	
ID-10-1		120–1700	PGM	
ID-11-1		60–1300	PGM	
ID-11-3		60–1300	SGM	
ID-12-2		170–1800	PGM	
ID-15-1		85–1600	PGM1	
ID-15-2		85–1600	PGM2	
D-01-1B		1700–10000	DCM, InSb(111), Si(111), Si(311), Si(422)	
D-11-1A		20–1900	PGM (SX-700)	
D-16-1a	30–1500	PGM variable deflection angle		
Advanced Light Source, Berkeley, California, USA	4.0.2	52–1900	Variable induced angle PGM	
	5.3.1	1800–12000	DCM, Si(111), Ge(111), InSb(111)	
	6.0.2	130–1800	VLS PGM	
	6.3.1	300–2000	VLS PGM	
	6.3.2	50–13000	VLS PGM	
	7.0.1	60–1200	SGM	
	7.3.1.1	175–1500	SGM	
	7.3.1.2	175–1500	SGM	
	8.0.1	65–1400	SGM	
	11.0.1	100–2000	VLS PGM	
	11.0.2	95–2000	Varied induced angle PGM	
	12.0.2	200–1000	VLSPGM	
	Swiss Light Source, Villigen, Switzerland	LUCIA	700–8000	DCM, YB ₆₆ , Beryl, InSb(111), Si(111)
SIM		90–2000	PGM (SX-700)	
Pohang Accelerator Laboratory, Pohang, Korea	2B1	12–1230	SGM	
	8A1	100–1600	PGM	
	2A1	90–1500	SGM, Dragon type	
	8C1	3000–22000	DCM, Si(111)	
	ELETTRA, Trieste, Italy	11.1	2300–25000	DCM Si(111), Si(311)
9.2		100–2000	PGM-SM, VLS/VLG	

Table 1 (continued)

Location	Beamline	Energy range (eV)	Monochromator optics
HASYLAB , Hamburg, Germany	A1	2400–17000	DCM Si(111)
	BW3	15–1800	PGM (SX-700)
	E4	2800–5000	DCM Si(111) with C mirror
Centre for Advanced Microstructures and Devices , Baton Rouge, USA	4A	25–1000	PGM
	5B	1000–15000	DCM
	Synchrotron Radiation Centre , Wisconsin, USA	HERMON	62–1100
National Synchrotron Light Source , Brookhaven National Laboratory, USA	041	75–2000	Multilayer monochromator
	051	250–2400	DCM, InSb(111), quartz(1010)
	093	1500–4000	SGM Grasshopper
	072	5–1200	SGM
	X1B	200–1600	DCM, Si(111), beryl(1010)
Advanced Photon Source , Illinois, USA	X8A	1000–5900	W/Si multilayer
	X15B	800–15000	DCM Si(111), Ge(111), Si(220), Si(311), InSb, beryl
	X19A	2100–17000	DCM, Si(111), Si(220), Si(311)
	X24A	1800–5000	DCM, Si(111), Ge(111), InSb,
	X24C	6–1800	Grating crystal monochromator
Advanced Photon Source , Illinois, USA	4-ID-C	500–2800	SGM
	9-BM	2100–30000	DCM, Si(111), Si(220)
	12-BM	2400–22000	DCM, Si(111)
	20-BM	2400–29000	DCM, Si(111)

YB₆₆ crystals are more resilient to radiation damage than quartz, beryl and α -SiO₂. The advantages of the YB₆₆ DCMs are offset by non-uniform crystal quality and crystal glitches (on wiggler and bending-magnet beamlines) at 1385.6 and 1436 eV (Kitamura *et al.*, 2003) that impinge on EXAFS spectra in this region. In the last 15 years, soft X-ray XAS has been ameliorated through progress in grating monochromator technology. Table 1 indicates that the overwhelming number of soft X-ray beamlines which cover the 1–2 keV energy range at major synchrotron facilities utilize grating monochromators. The two main classes of grating monochromator design that operate over this energy range are: (i) spherical-grating monochromators (SGM) and (ii) plane-grating monochromators (PGM). The seminal high-resolution grating monochromator was based on a spherical-grating geometry (Chen & Sette, 1989). Subsequently, advances in the instrumental geometry required to achieve high spectral resolution from dispersive optics has resulted in the ubiquitous use of plane- and spherical-grating monochromators in soft X-ray (less than 2 keV) beamlines.

8. Conclusions

Bioinorganic chemical knowledge grows more interesting and more complex with each passing year. Remarkably, more details about the usage and utility of inorganic species, alkaline and alkaline earth metal ions in biological species and bioinorganic molecules become available. Yet, structure–function investigations of naturally occurring inorganic centers are not trivial. Here we have reviewed the advantages as well as the difficulties associated with the application of softer bioXAS to probe the local structural and electronic

environments of low-*Z* inorganic elements within their biological complexes. Developments in the fields of beamline design, detectors, sample preparation and bioXAS data analysis hold the promise to advance our ability to study such reactive centers in dilute samples and biological systems.

Research at the University of Saskatchewan was supported in part by a Canada Research Chair award (GNG), the University of Saskatchewan, the Province of Saskatchewan, the National Institutes of Health (GM5735), the Natural Sciences and Engineering Research Council (Canada) (283315) and the Canadian Institute of Health Research. The Stanford Synchrotron Radiation Laboratory is funded by the US Department of Energy, Office of Basic Energy Sciences and Office of Biological and Environmental Sciences, and the National Institutes of Health, National Center for Research Resources. Research at the Weizmann Institute is supported by the Minerva foundation, ISF and HFSP.

References

- Barondeau, D. P. & Getzoff, E. D. (2004). *Curr. Opin. Struct. Biol.* **14**, 765–774.
- Beinert, H. (2000). *Eur. J. Biochem.* **26**, 5657–5664.
- Bunick, C., Nelson, M. R., Mangahas, S., Hunter, M. J., Sheehan, J. H., Mizoue, L. S., Bunick, G. J. & Chazin, W. J. (2004). *J. Am. Chem. Soc.* **126**, 5990–5998.
- Cech, T. R. (2002). *Biochem. Soc. Trans.* **30**, 1162–1166.
- Chen, C. T. & Sette, F. (1989). *Rev. Sci. Instrum.* **60**, 1616.
- Cheung, K. C., Strange, R., Harvey, I., Dobson, B., Derbyshire, G., Kay, J., Binsted, N., Linford, R. & Hasnain, S. S. (1999). *J. Synchrotron Rad.* **6**, 161–163.
- Cheung, K. C., Strange, R. W. & Hasnain, S. S. (2000). *Acta Cryst.* **D56**, 697–704.
- Claiborne, A., Yeh, J. I., Mallett, T. C., Luba, J., Crane, E. J. III, Charrier, V. & Parsonage, D. (1999). *Biochemistry*, **38**, 15407–15416.
- Collins, C. A. & Guthrie, C. (2000). *Nature Struct. Biol.* **7**, 850–854.
- Delhaize, E., Rayen, R. P., Hebb, D. M., Yamamoto, Y., Sasaki, T. & Matsumoto, H. (2004). *Proc. Natl. Acad. Sci. USA*, **101**, 15249–15254.
- Denli, A. M. & Hannon, G. J. (2003). *Trends Biochem. Sci.* **28**, 196–201.
- Dey, A., Glaser, T., Couture, M., Moura, J. J.-G., Eltis, L. D., Holm, R. H., Hedman, B., Hodgson, K. O. & Solomon, E. I. (2004). *J. Am. Chem. Soc.* **126**, 8320–8328.
- Draper, D. E. (2004). *RNA*, **10**, 335–343.
- Faustino, N. A. & Cooper, T. A. (2003). *Genes Dev.* **17**, 419–437.
- Fischetti, R., Stepanov, S., Rosenbaum, G., Barrea, R., Black, E., Gore, D., Heurich, R., Kondrashkina, E., Kropf, A. J., Wang, S., Zhang, K., Irving, T. C. & Bunker, G. B. (2004). *J. Synchrotron Rad.* **11**, 399–405.
- Flendrig, J. A., Kruis, H. & Das, H. A. (1976). *Lancet*, **1**, 1235.
- Frank, P., Hedman, B. & Hodgson, K. O. (1999). *Inorg. Chem.* **38**, 260–270.

- Friedrich, S., Mears, C. A., Niderost, B., Hiller, L. J., Frank, M., Labov, S. E., Barfknecht, A. T. & Cramer, S. P. (1998). *Microsc. Microanal.* **4**, 616–621.
- Galburt, E., Chevalier, B., Tang, W., Jurica, M. S., Flick, K. E., Monnat, R. J. Jr & Stoddard, B. L. (1999). *Nature Struct. Biol.* **6**, 1096–1099.
- George, G. N., Garrett, R. M., Prince, R. C. & Rajagopalan, K. V. (1996). *J. Am. Chem. Soc.* **118**, 8588–8592.
- George, G. N. & Gorbaty, M. L. (1989). *J. Am. Chem. Soc.* **111**, 3182–3186.
- George, G. N., Pickering, I. J., Yu, E. Y., Prince, R. C., Bursakov, S. A., Gavel, O. Y., Moura, I. & Moura, J. J. G. (2000). *J. Am. Chem. Soc.* **122**, 8321–8322.
- Gesteland, R. F., Cech, T. R. & Atkins, J. F. (1999). *The RNA World*. New York: Cold Spring Harbor Laboratory.
- Harris, H. H., Pickering, I. J. & George, G. N. (2003). *Science*, **381**, 1203.
- Henn, A., Medalia, O., Shi, S. P., Steinberg, M., Franceschi, F. & Sagi, I. (2001). *Proc. Natl. Acad. Sci. USA*, **98**, 5007–5012.
- Henn, A., Shi, S. P., Zarivach, R., Ben-Zeev, E. & Sagi, I. (2002). *J. Biol. Chem.* **277**, 46559–46565.
- Herschlag, D. (1995). *J. Biol. Chem.* **270**, 20871–20874.
- Hirsch, E. C., Brandel, J. P., Galle, P., Javoy-Agid, F. & Agid, Y. (1991). *J. Neurochem.* **56**, 446–451.
- Jellinger, K. A. & Bancher, C. (1998). *J. Neural. Transm. Suppl.* **54**, 77–95.
- Johnson, W. C. Jr (1992). *Methods Enzymol.* **210**, 426–447.
- Julka, D., Vasishta, R. K. & Gill, K. D. (1996). *Biol. Trace Elem. Res.* **52**, 181–192.
- Kitamura, M., Yoshikawa, H., Tanaka, T., Mochizuki, T., Vlaicu, A. M., Nisawa, A., Yagi, N., Okui, M., Kimura, M. & Fukushima, S. (2003). *J. Synchrotron Rad.* **10**, 310–312.
- Kleinfeld, O., Frenkel, A., Martin, J. M. & Sagi, I. (2003). *Nature Struct. Biol.* **10**, 98–103.
- Klein, D. J., Moore, P. B. & Steitz, T. A. (2004). *RNA*, **10**, 1366–1379.
- Kochian, L. V. (1995). *Annu. Rev. Plant Physiol. Mol. Biol.* **46**, 237–260.
- Lorsch, J. R. (2002). *Cell*, **109**, 797–800.
- MacKinnon, R. (2004). *Angew. Chem. Int. Ed. Engl.* **43**, 4265–4277.
- Massova, I., Kotra, L. P. & Mobashery, S. (1998). *Bioorg. Med. Chem. Lett.* **8**, 853–858.
- Matsumoto, H. (2000). *Int. Rev. Cytol.* **200**, 1–46.
- Milligan, J. F., Groebe, D. R., Witherell, G. W. & Uhlenbeck, O. C. (1987). *Nucl. Acids Res.* **15**, 8783–8789.
- Misra, V. K. & Draper, D. E. (1998). *Biopolymers*, **48**, 113–135.
- Morra, M. L., Fendorf, S. E. & Brown, P. D. (1997). *Geochim. Cosmochim. Acta*, **61**, 683–688.
- Nakano, S., Proctor, D. J. & Bevilacqua, P. C. (2001). *Biochemistry*, **40**, 12022–12038.
- Penner-Hahn, J. E. (2004). *Coord. Chem. Rev.* **249**, 161–177.
- Piccirilli, J. A., Vyle, J. S., Caruthers, M. H. & Cech, T. R. (1993). *Nature Rev.* **361**, 85–88.
- Pickering, I. J., George, G. N., Van Fleet-Stalder, V., Chasteen, T. G. & Prince, R. C. (1999). *J. Biol. Inorg. Chem.* **4**, 791–794.
- Pickering, I. J., George, G. N., Yu, E. Y., Brune, D. C., Tuschak, C., Overmann, J., Beatty, J. T. & Prince, R. C. (2001). *Biochemistry*, **40**, 8138–8145.
- Pickering, I. J., Prince, R. C., Divers, T. & George, G. N. (1998). *FEBS Lett.* **441**, 11–14.
- Pyle, M. A. (2002). *J. Biol. Inorg. Chem.* **7**, 679–690.
- Raines, R. T. (1997). *Nature Struct. Biol.* **4**, 424–427.
- Rocak, S. & Linder, P. (2004). *Nature Rev.* **5**, 232–241.
- Schiemann, O., Fritscher, J., Kisseleva, N., Sigurdsson, S. T. & Prisner, T. F. (2003). *ChemBiochemistry*, **4**, 1057–1065.
- Shadle, S. E., Penner-Hahn, J. E., Schugar, H. J., Hedman, B., Hodgson, K. O. & Solomon, E. I. (1993). *J. Am. Chem. Soc.* **115**, 767–776.
- Sneed, E. Y., Harris, H. H., Pickering, I. J., Prince, R. C., Johnson, S., Li, X., Block, E. & George, G. N. (2004). *J. Am. Chem. Soc.* **126**, 458–459.
- Solomon, E. I., Hedman, B., Hodgson, K. O., Dey, A. & Szilagyi, R. K. (2005). *Coord. Chem. Rev.* **249**, 97–129.
- Steitz, T. A. & Moor, P. B. (2003). *Trends Biochem. Sci.* **28**, 411–418.
- Stiefel, E. I. (1996). *Transition Metal Sulfur Chemistry, Biological and Industrial Significance*, edited by E. I. Stiefel and K. Matsumoto. Preface. Washington, DC: American Chemical Society.
- Su, L. J., Brenowitz, M. & Pyle, A. M. (2003). *J. Mol. Biol.* **334**, 639–652.
- Toimela, T. & Tahti, H. (2004). *Arch. Toxicol.* **78**, 565–574.
- Toohey, J. I. (1989). *Biochem. J.* **264**, 625–632.
- Toyoshima, C., Nomura, H. & Tsuda, T. (2004). *Nature (London)*, **432**, 361–368.
- Treiber, D. K. & Williamson, J. R. (1999). *Curr. Opin. Struct. Biol.* **9**, 339–345.
- Uexkull, H. R. von & Mutert, E. (1995). *Plant Soil*, **171**, 1–15.
- Vairavamurthy, A., Zhou, W., Eglinton, T. & Manowitz, B. (1994). *Geochim. Cosmochim. Acta*, **58**, 4681–4687.
- Williams, K. R., Gamelin, D. R., LaCroix, L. B., Houser, R. P., Tolman, W. B., Mulder, T. C., de Vries, S., Hedman, B., Hodgson, K. O. & Solomon, E. I. (1997). *J. Am. Chem. Soc.* **119**, 613–614.
- Wong, J., George, G. N., Pickering, I. J., Rek, Z. U., Rowen, M., Tanaka, T., DeVries, B., Vaughan, D. E. W., Via, G. H. & Brown, G. E. Jr (1994). *Solid State Commun.* **92**, 559–562.
- Woodson, S. A. (2000). *Cell. Mol. Life Sci.* **5**, 796–808.
- Yasui, M., Yase, Y., Ota, K. & Garruto, R. M. (1991). *Neurotoxicology*, **12**, 615–620.
- Yogeewari, P., Ragavendran, J., Thirumurugan, R., Saxena, A. & Sriram, D. (2004). *Curr. Drug Targets*, **5**, 589–602.
- Yomoto, S., Nagi, J., Imamura, M., Matsuzaki, H., Hayashi, K., Matsuda, A., Kumazawa, H., Ohashi, H. & Kobayashi, K. (1997). *Nucl. Instrum. Methods Phys. Rev. B*, **12**, 615–620.
- Yu, E. Y., Pickering, I. J., George, G. N. & Prince, R. C. (2001). *Biochim. Biophys. Acta*, **152**, 156–160.